

RXTE and ASCA Constraints on Non-thermal Emission from the A2256 Galaxy Cluster

Mark Henriksen

Physics Department, University of North Dakota, Grand Forks, ND 58202-7129
 mahenrik@plains.NoDak.edu

ABSTRACT

An 8.3 hour observation of the Abell 2256 galaxy cluster using the Rossi X-ray Timing Explorer (RXTE) proportional counter array (PCA) produced a high quality spectrum in the 2 - 30 keV range. Joint fitting with the 0.7 - 11 keV spectrum obtained with the Advanced Satellite for Astrophysics and Cosmology (ASCA) Gas Imaging spectrometer (GIS) gives an upperlimit of $\sim 2.3 \times 10^{-7}$ photons $\text{cm}^{-2} \text{sec}^{-1} \text{keV}^{-1}$ for non-thermal emission at 30 keV. This yields a lower limit to the mean magnetic field of $0.36 \mu\text{G}$ and an upperlimit of 1.8×10^{-13} ergs cm^{-3} for the cosmic-ray electron energy density. The resulting lower limit to the central magnetic field is $\sim 1 - 3 \mu\text{G}$. While a magnetic field of $\sim 0.1 - 0.2 \mu\text{G}$ can be created by galaxy wakes, a magnetic field of several μG is usually associated with a cooling flow or, as in the case of the Coma cluster, a subcluster merger. However, for A2256, the evidence for a merger is weak and the main cluster shows no evidence of a cooling flow. Thus, there is presently no satisfactory hypothesis for the origin of an average cluster magnetic field as high as $> 0.36 \mu\text{G}$ in the A2256 cluster.

Subject headings: galaxies: clusters: individual (A2256) – galaxies: intergalactic medium
 – galaxies: magnetic fields – X-rays: galaxies

1. Introduction

The Abell 2256 galaxy cluster ($z = 0.058$), like the Coma cluster, is one of the most studied galaxy clusters. A2256 and the Coma cluster share many common properties: they have similar X-ray luminosities, both have optical and X-ray substructure, and both have a radio halo. As with Coma, it has been over 20 years since the radio halo of A2256 was discovered (Bridle & Fomalont 1976; Bridle et al. 1979). These authors report that the radio halo has a flux of 0.1 Jy at 610 MHz and extends to a radius of 5 arcmin or $0.52H_0^{-1}$ Mpc. The spectrum is a powerlaw given by, $S = 6.5 \times 10^{-9} \nu^{-1.8}$ ergs cm^{-2} $\text{sec}^{-1} \text{Hz}^{-1}$. The spectral index is determined between 610 and 1415 MHz. As with Coma, the radio spectrum is attributed to synchrotron emission from a population of relativistic electrons interacting with a diffuse intergalactic magnetic field. Recent studies of the Coma cluster link the X-ray and radio emission to support the hypothesis that the merger amplifies the magnetic field. However, for A2256 this hypothesis may not work since the evidence for a merger is incomplete; there is evidence of substructure, yet shock heating due to the merger is not apparent in the temperature map obtained with *ASCA* (Markevitch & Vikhlinin 1997) as it is for Coma.

X-ray emission is also expected from inverse-Compton scattering of cosmic microwave photons off of the relativistic electrons which produce the radio halo. So far, attempts to detect non-thermal emission have only produced upper limits for both clusters. Previous searches for non-thermal emission from A2256 have utilized hard X-ray data obtained with HEAO1-A4 (Rephaeli, Gruber, & Rothschild 1987). An upper limit to the non-thermal X-ray flux reported from this study is 5×10^{-6} photons cm^{-2} sec^{-1} keV^{-1} at 30 keV. The lower limit to the average magnetic field of A2256 is 0.11 μG .

The alternative hypothesis to mergers, that galaxy wakes amplify a seed field, leads to an average field in the range of 0.1 - 0.2 μG (Goldman & Rephaeli 1991). If this hypothesis is correct, non-thermal emission should be detectable for A2256 with even a slight improvement in sensitivity over the HEAO-1 A4 X-ray spectrum. In this paper, we use the very high signal to noise data obtained with the *ASCA* GIS combined with that obtained with the *RXTE* PCA to place a more sensitive limit on the non-thermal X-ray emission from the A2256 cluster. This new limit

provides a more stringent constraint on current hypotheses for its origin. A value of 50 $\text{km s}^{-1} \text{Mpc}^{-1}$ is used throughout this paper.

2. Observations

The Abell 2256 cluster was observed with *RXTE* on 1997 June 24-26 for 30,000 seconds. Data obtained with the PCA is analyzed and presented here. The PCA consists of five proportional counter units (PCU), each of which contains three detector layers. The nominal energy band of the PCA is 2 - 60 keV. After filtering the PCA data, there were $\sim 22,000$ seconds of good data. Filtering involved excluding data when less than 5 PCUs were on (this eliminated < 1000 seconds), excluding data taken when the pointing was > 0.02 degrees offset from the source, excluding data taken < 10 degrees elevation from the Earth, excluding times near passage through the South Atlantic Anomaly which showed large variations in the count rate. The observation was carried out in two observing periods, each resulting in $\sim 11,000$ seconds of filtered data. Three *RXTE* spectra were modeled: that obtained for the top layer detectors alone for each observation period, both separate and combined, and the top and middle layer detectors. The background was modeled using the latest models available from the *RXTE* Guest Observer Facility. The background estimation is based on three models: VLE, activation, and cosmic X-ray background. The VLE (based on the rate of Very Large Event discriminator) background results from interaction of cosmic-rays with the spacecraft or detector and unvetted cosmic-ray tracks. The activation model depends on orbital coordinates and corrects for additional background associated with passes from the South Atlantic Anomaly. The cosmic X-ray background component is derived from blank sky observations taken in 1997 to give an average high-latitude X-ray background spectrum.

The model background consists of the VLE and activation components (in which sky background is included from blank sky observations). In the third layer, in the 30 - 60 keV range, little source emission should be present. Indeed, the count rate in the 2 - 30 keV range between the first and second layer drops by a factor of ~ 15 and the ~ 7 keV thermal continuum which characterizes the A2256 X-ray spectrum contributes little emission above 30 keV. The model background is fit to the 30 - 60 keV spectrum, while normalizing the activation component separately to

minimize χ^2 .

The 2 - 30 keV part of the spectrum used in the model fitting utilizes the background derived by this procedure. The best constraint on the non-thermal flux was obtained fitting data obtained in the top and second layers in the first 11 ksec observing period. The background subtracted count rates for the data analyzed are: 28.43 ± 0.23 counts sec^{-1} in the top layer of the PCA, 1.91 ± 0.07 counts sec^{-1} in the second layer, and 1.16 ± 0.05 counts sec^{-1} in the third layer.

The spectral response of the PCA depends on the overall gain setting, which PCUs are analyzed since they have different gains, and the detector layer. Separate response matrices were created for each detector layer of each PCU used. The matrices were binned to the 129 channel, standard 2 configuration in which the data were analyzed. There is a feature in the response from the detector due to the Xenon L edge at 4.78 keV which produces an absorption feature in the spectrum. Ignoring channels 10 - 11 in the PCA greatly reduces the residuals in this part of the spectrum; this is done in all of the model fitting which involves the PCA.

The *ASCA* GIS spectrum consists of 34,726 seconds of good data with a count rate of 1.57 ± 0.007 counts s^{-1} . Preparation of the GIS spectrum and related calibration issues are discussed in detail in Henriksen (1998).

3. Analysis and Results

The models fit to the data consist of one or two Raymond & Smith (RS) (1977) thermal components with and without a power law component. For the thermal components, all data groups share the following free parameters: column density, temperature, and abundance. The normalization(s) for the PCA data sets are tied while the GIS has its own normalization(s). The powerlaw component has a free normalization and the spectral index is fixed at the photon index measured from the radio, 2.8, which is also the spectral index of the inverse-Compton component. Both the GIS and the PCA field of view contain the region of the radio halo so their powerlaw normalizations are tied. Thus, for the joint data fits, there are 6 free parameters for the single RS component plus a powerlaw and 8 free parameters for the model consisting of 2 RS components and a powerlaw. The 90% range on fit parameters are given in Tables 1 and 2 for each data set alone and the joint fit.

When addition of a powerlaw improves χ^2 , the fit is also shown without the powerlaw to make the significance of the additional component apparent.

The addition of a second temperature component is significant using the PCA data alone as well as in the joint fit which uses both the PCA and GIS data. This is not a surprising feature of the integrated spectrum since a temperature map of the cluster shows multiple components (Markevitch & Vikhlinin 1997; Miyaji et al. 1993). The addition of the second, cooler component provides much improvement in the joint fit; $\Delta\chi^2$ decreases by 60 for 3 additional degrees of freedom. The parameters derived from fitting the GIS data and the PCA data separately are in very good agreement, suggesting the data are independently well calibrated. The PCA data alone do not constrain the Galactic column density so this parameter is tied at the value measured from neutral hydrogen, 4.2×10^{20} .

The PCA data alone is consistent with a detection of non-thermal emission when a powerlaw is added to a single thermal component. However, addition of a second thermal component rather than the powerlaw provides an even better fit to the data. Addition of a powerlaw to the two thermal components then degrades the fit and the data provide an upper limit on non-thermal emission. The joint fit with the GIS also shows that a second thermal component provides a much better fit than does a powerlaw. The joint fit of a 2 RS model also then gives the best upper limit on non-thermal emission. The upperlimit on the non-thermal flux obtained from the joint fit, 2.64×10^{-12} ergs $\text{cm}^{-2} \text{s}^{-1}$ in the 2 - 10 keV band is ~ 24 times better than that obtained by *HEAO1-A4*. The best fit two RS model with a powerlaw set at the 90% upperlimit is shown in Figure 1.

The *RXTE* PCA temperature alone is 6.63 - 6.81 keV, in good agreement with the *ASCA* GIS, 6.78 - 7.44 keV, and measurements by previous X-ray observations: the *Einstein* MPC (6.7 - 8.1 keV; David et al. 1993), and *GINGA* (7.32 - 7.70 keV; Hatsukade 1989). The abundance obtained from *RXTE*, 0.15 - 0.18 is consistent with *ASCA*, 0.16 - 0.24. This general agreement with past measurements suggests that the spectral calibration of the PCA is accurate within the energy band used here.

4. Calculation of $\langle B \rangle$ and U_r

The average magnetic field, $\langle B \rangle$, is calculated from the radio spectrum and the X-ray flux

TABLE 1
RESULTS OF SINGLE AND JOINT FITS

Model	Data Set	$n_H \times 10^{22} \text{cm}^{-2}$	kT(keV)	Abundance	NT Normalization ^a	χ^2/dof
1RS	GIS	0.028 - 0.061	6.78 - 7.44	0.16 - 0.24	<0.0045	633.0/604
1RS	PCA	0.042 ^b	6.63 - 6.81	0.15 - 0.18	-	172.6/114
1RS + POW	PCA	0.042 ^b	7.10 - 7.43	0.23 - 0.27	0.0091 - 0.015	127.6/113
1RS	Joint	0.042 - 0.066	6.66 - 6.84	0.16 - 0.18	-	815.8/720
1RS + POW	Joint	0.091 - 0.18	6.79 - 7.08	0.18 - 0.22	0.0019 - 0.0087	806.7/719
2RS	PCA	0.042 ^b	6.97 - 7.59	0.18 - 0.24	<0.0082	122.5/113
			0.71 - 1.71			
2RS	Joint	0.029 - 0.11	6.99 - 7.38	0.19 - 0.23	<0.0032	756.0/717
			0.75 - 1.46			

^aNon-thermal upperlimit in photons $\text{cm}^{-2}\text{s}^{-1}\text{keV}^{-1}$ at 1 keV

^b n_H fixed at the Galactic value, 0.042

TABLE 2
RESULTS OF JOINT FITS

Model	Data Set	Norm: High T	Norm: Low T	Flux: High T ^a	Flux: Low T ^a
1RS	GIS	0.087 - 0.089	-	7.81	-
-	PCA	0.071 - 0.073	-	6.36	-
1RS + POW	GIS	0.078 - 0.085	-	6.89	-
-	PCA	0.063 - 0.066	-	5.78	-
2RS	GIS	0.084 - 0.087	0.00 - 0.011	7.97	0.00
-	PCA	0.063 - 0.068	0.024 - 0.077	6.12	0.31

^a $\times 10^{-11} \text{ergs cm}^{-2}\text{s}^{-1}\text{keV}^{-1}$ in 2 - 10 keV band. Flux is derived from best fitting normalization.

upperlimit using the equations in Henriksen (1998). This procedure combines the expressions for the synchrotron flux and the Compton flux to eliminate the relativistic electron density to obtain an expression which is independent of the size of the emitting region or the distance to the cluster. The derived values of $\langle B \rangle$ are given in Table 3.

The highest lower limit is $0.36\mu\text{G}$. An upperlimit to the energy density of relativistic electrons is calculated using the following equation:

$$U_r = C \int (\gamma E) \gamma^{-p} d\gamma. \quad (1)$$

In this equation, U_r is the relativistic electron energy density, γ is the Lorentz factor, E is the electron rest energy, and C and p are defined by the relativistic electron density distribution,

$$n(\gamma) = C\gamma^{-p}. \quad (2)$$

The lower limit on the integral is the minimum γ needed to boost a CMBR photon to the X-ray regime, 1000. Solving the integral gives,

$$U_r = \frac{CE\gamma_{min}^{2-p}}{p-2}. \quad (3)$$

The spectral index of the relativistic electrons (p) is related to the photon index used to model the inverse-Compton emission ($\alpha_x = 2.8$) by $p = 2\alpha_x - 1$. The parameter C is calculated by multiplying equation (4) in Henriksen (1998), which is the expression for the inverse-Compton energy density in terms of various constants, by the volume containing the relativistic electrons which is taken to be a sphere with radius equal to that of the radio halo. This equation is then divided by $4\pi D^2$, where D is the distance to the cluster to get the inverse-Compton flux. The inverse-Compton flux, given in Table 3 in the 2 - 10 keV energy band is the primary observational constraint in this calculation. The calculated upper limits on U_r are given in Table 3. The magnetic field energy density is calculated for comparison and shown in Table 3. In all cases, the energy density in cosmic rays and the magnetic field are consistent with equipartition.

5. Discussion

A joint fit of the GIS and PCA data in the 0.7 - 30 keV band show that the A2256 spectrum is best described by a model consisting of 2 thermal components. Using a single thermal component leads to a

detection of non-thermal emission. However, a second thermal component provides a better description of the data and obviates the need for non-thermal emission. These data place a more stringent upper limit on the flux of non-thermal emission, $<2.64 \times 10^{-12}$ ergs $\text{cm}^{-2} \text{s}^{-1}$ in the 2 - 10 keV band, or $<4\%$ of the thermal component. From the upper limit on non-thermal emission, a lower limit to the average magnetic field is calculated, $>0.36 \mu\text{G}$. If the field is assumed to be frozen into the intracluster gas, then the central field will be higher. Using the gas density parameters for A2256 (Jones and Forman 1984) and the formulae in Goldshmidt and Rephaeli (1994), a central field of $\gtrsim 1 - 3 \mu\text{G}$ is calculated. The range corresponds to using the radio halo or the intracluster medium for the average magnetic field extent. Using these parameters (central gas density = $2.5 \times 10^{-3} \text{cm}^{-3}$) and the ambient gas temperature of 7 keV gives a central gas energy density of 3×10^{-11} ergs cm^{-3} . The highest lower limit to the magnetic field energy density at the center, $>3.6 \times 10^{-13}$, is almost a factor of ~ 83 lower. The energy density in cosmic-ray electrons, $<1.8 \times 10^{-13}$, is also much lower. This gives an indication of the relative importance of the magnetic field and cosmic-ray electrons on the gas dynamics of the cluster. The cosmic-ray energy is not significant. The magnetic field energy is a lower limit and not constraining. Detection of an average magnetic field which gives a comparable energy density to the gas at the center would require an increase in sensitivity in X-ray flux of ~ 470 .

The hypothesis that galaxy wakes amplify a seed field via the dynamo process leads to an average field of 0.1 - 0.2 μG (Goldman & Rephaeli 1991). These authors use a lower, more realistic efficiency for the conversion of kinetic energy into magnetic field energy than earlier studies which produced a field of $\sim 2 \mu\text{G}$ (Ruzmaikin, Sokoloff, & Shukarov 1989). Amplification for seed fields has also been considered by De Young (1992) using time-dependent evolution of magnetohydrodynamic turbulence from galaxy wakes. He found that amplification to a few μG with this mechanism is very rare. Magnetic field strengths of a few μG have previously been inferred from studies of the excess rotation measure (RM) (Kim et al. 1990; Crusius-Watzel et al. 1990; Kim, Kronberg, & Tribble 1991) in galaxy clusters. Though these high magnetic fields challenge the hypothesis of wake amplification, they are more model dependent as they are sensitive to local density inhomogeneities or an asymmetric gas

TABLE 3
CALCULATED PARAMETERS

Model	Data Set	NT Flux ^a	 μ G	U _r ^b	U _B ^c
1RS	GIS	<3.64	>0.30	<2.55	>3.58
	PCA	7.5 - 12.5	0.20 - 0.25	5.3 - 8.6	1.6 - 2.5
	Joint	1.58 - 7.09	0.25 - 0.43	1.1 - 5.0	2.5 - 7.4
2RS	PCA	<6.80	>0.25	<4.8	>2.5
	Joint	<2.64	>0.36	<1.8	>5.2

^aNon-thermal flux: $\times 10^{-12}$ ergs cm⁻²s⁻¹ in 2 - 10 keV band

^bElectron energy density: $\times 10^{-13}$ ergs cm⁻³

^cMagnetic field energy density: $\times 10^{-15}$ ergs cm⁻³

distribution. Clusters often have both due to accretion of groups and subcluster mergers. In addition, many other clusters also have cooling flows which can amplify the magnetic field through isotropic compression (Soker & Sarazin 1990; Tribble 1991). The distribution of excess rotation measures for Abell clusters found by Kim et al. is consistent with amplification by galaxy wakes if $\sim 10\%$ have cooling flows which further amplify the magnetic fields (Carvalho 1994). However, this requires that clusters with the larger magnetic fields, $>0.1 - 0.2 \mu$ G, be those clusters with cooling flows. Based on a deprojection analysis of its X-ray emission, A2256 does not have a cooling flow (Stewart et al. 1984) and does not show the surface brightness central excess which is typical of clusters with cooling flows (Jones & Forman 1984).

As an alternative, Tribble (1993) has suggested that cluster mergers have amplified the magnetic fields in clusters with radio halos. This hypothesis has received support in subsequent studies of the radio halo in Coma which suggest that it may be maintained by the recent merger experienced in the cluster center which is apparent in the X-ray (Deiss et al. 1997). Bohringer et al. (1992) find that the available energy specifically from the accretion of groups near the core may be enough to reaccelerate cosmic-ray electrons and amplify the magnetic field to maintain the halo. However, this hypothesis presents a problem in the case of A2256 because the evidence for a merger is controversial. The pattern of heating expected in a merger has been found in several of the clusters (Coma, A754, and A1367). Non-isothermality in the atmosphere of A2256 was

reported using *ROSAT* PSPC data (Briel & Henry 1994), *BBXRT* data (Miyaji et al. 1993), and *ASCA* Markevitch & Vikhlinin (1997). However, the latter author's found that the temperature map was consistent with the superposition of two subclusters with different temperatures rather than a merger. Future observation of A2256 by the Advanced X-ray Astrophysics Facility (AXAF) will likely provide a more definitive description of the dynamical state of the cluster. Thus, a satisfactory hypothesis for the origin of an average magnetic field $> 0.4 \mu$ Gauss in A2256 is not yet apparent.

I thank the National Science Foundation for supporting this research. I also thank the referee for comments on improving this manuscript.

REFERENCES

- Bohringer, H., Schwarz, R., Briel, U., Voges, W., Ebeling, H.; Hartner, G.; Cruddace, R., 1992, in *Clusters and Superclusters of Galaxies*: ed. A. Fabian, (NATO/ASI), 71
- Briel, U., and Henry, J., 1994, *Nature*, 372, 439
- Bridle, A., & Fomalont, E., 1976, *A&A*, 52, 107
- Bridle, A., Fomalont, E., Miley, G., Valentijn, 1979, *A&A*, 80, 201
- Carvalho, J.C. 1994, *A&A*, 281, 641
- Crusius-Watzel, A., Biermann, P., Lerche, I., & Schlickeiser, R. 1990, *ApJ*, 360, 417

- David, L.P., Slyz, A., Jones, C., Forman, W. Vrtilek, S.D., Arnaud, K.A., 1993, ApJ, 412, 479.
- Deiss, B., Reich, W., Lesch, H., and Wielebinski, R., 1997, A&A, 321, 55
- De Young, D., 1992, ApJ, 386, 464
- Goldman, I., Rephaeli, Y., 1991, ApJ, 380
- Goldshmidt, O., and Rephaeli, Y., 1994, ApJ, 431, 586
- Hatsukade, I., 1989, Ph.D. Thesis, Osaka University
- Henriksen, M., 1998, PASJ, 50, (in press)
- Jones, C., and Forman, W., 1984, ApJ, 276, 38
- Kim, K.-T., Kronberg, P.P., Dewdney, P.E., Landecker, T.L., 1990, ApJ, 355, 29
- Kim, K. -T., Kronberg, P. P., Tribble, P. C., 1991, ApJ, 379, 80
- Markevitch, M., & Vikhlinin, A., 1997, ApJ, 474, 84
- Miyaji, T., et al., 1993, ApJ, 419, 66
- Raymond, J., and Smith, B., 1977, ApJS, 35, 419
- Rephaeli, Y., Gruber, D., & Rothschild, R., 1987, ApJ, 320, 139
- Ruzmaikin, A., Sokoloff, D., Shukarov, A., 1989, MNRAS, 241, 1
- Soker, N., and Sarzin, C., 1990, ApJ, 348, 73
- Stewart, G., Fabian, A., Jones, C., Forman, W., 1984 ApJ, 285 1
- Tribble, P. 1991, MNRAS, 248, 741
- Tribble, P. 1993, MNRAS, 263, 31

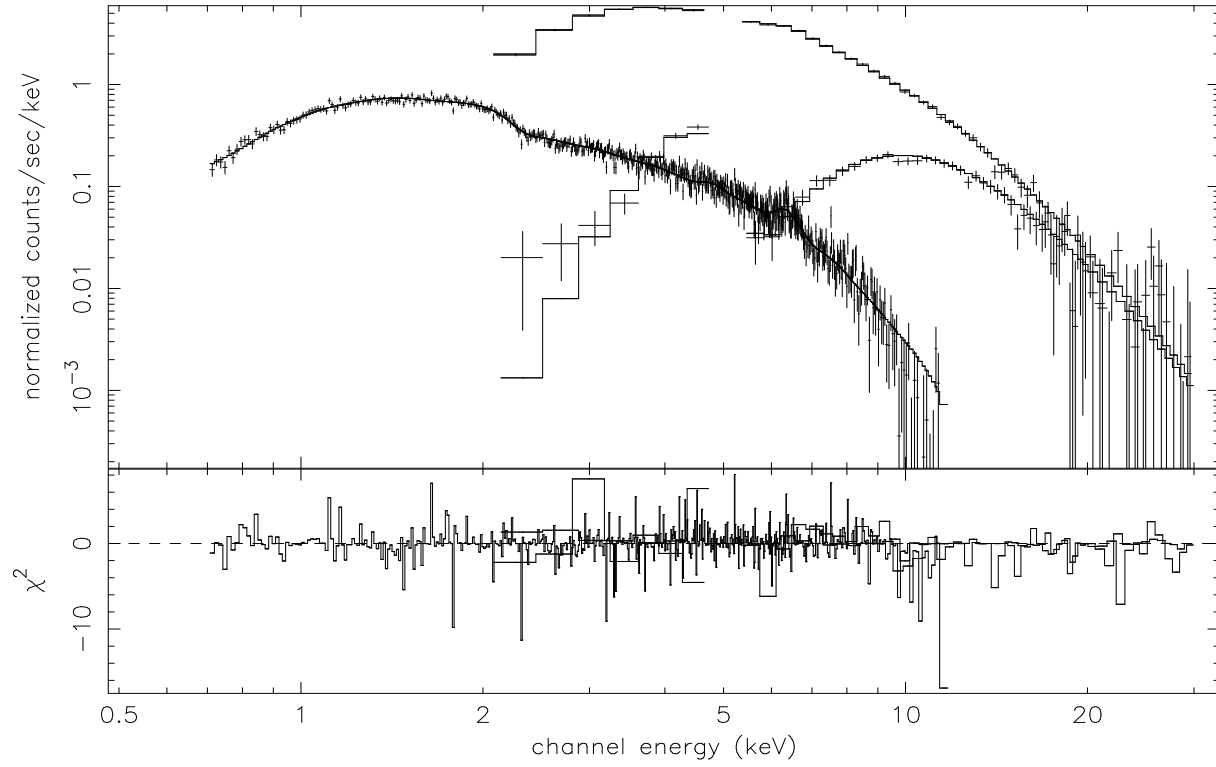


Fig. 1.— Best fit model for joint fit to ASCA GIS and RXTE PCA data shown with a powerlaw component added at the 90% confidence upperlimit.